HortScience 59(5):595–604. 2024. https://doi.org/10.21273/HORTSCI17669-23

Root System Reductions of Grafted 'Valencia' Orange Trees Are More Extensive Than Aboveground Reductions after Natural Infection with *Candidatus* Liberibacter Asiaticus

Caroline Tardivo
University of Florida/Institute of Food and Agricultural Sciences, Southwest Florida Research and Education Center, Immokalee, FL 34142, USA

Leigh Archer
University of Florida/Institute of Food and Agricultural Sciences, Southwest Florida Research and Education Center, Immokalee, FL 34142, USA; and Rodale Institute, Kutztown, PA 19530, USA

Larissa Nunes, Fernando Alferez, and Ute Albrecht
University of Florida/Institute of Food and Agricultural Sciences, Southwest Florida Research and Education Center, Immokalee, FL 34142, USA

Keywords. citrus greening, excavation, fibrous roots, individual protective covers, phloem pathogen

Abstract. **Huanglongbing (HLB), which is associated with the phloem-limited bacteria *Candidatus* Liberibacter asiaticus (*C*Las), is a devastating disease that affects citrus trees worldwide. Because of the pervasiveness of the bacteria and psyllid vector, the disease is considered endemic in Florida. Although the effects of *C*Las on tree growth and physiology have been investigated for decades, most studies compared infected and noninfected trees under greenhouse conditions. This study used newly planted field-grown 'Valencia' sweet orange (*Citrus sinensis*) trees on two different rootstocks to monitor the distribution and accumulation of *C*Las in aboveground and belowground tissues following natural psyllid colonization and assess tree physiological responses and biomass reductions under HLB-endemic conditions. Trees were transplanted into the field with individual protective covers (IPCs), which are used to exclude psyllids and prevent infection. Openings were cut in the IPCs of half of the trees; to promote infection, these IPCs were temporarily removed during the main vegetative flushing period when psyllid populations were high. All trees that were exposed to psyllids became infected and displayed the symptoms typically associated with HLB. Throughout the study, higher levels of *C*Las were detected in the leaves compared with those in the fibrous roots. Trees that were not exposed to psyllids remained noninfected and healthy. After 18 months, a subset of trees was excavated to assess biomass differences between infected and noninfected trees. Infected trees had root system reductions of 37% and shoot system reductions of 20%, thereby significantly reducing the belowground-to-aboveground biomass ratio. Fibrous root loss was 49% and more severe than the loss of the rest of the root tissue. This study is the first to demonstrate the full extent of damage caused by *C*Las infection under natural HLB-endemic conditions. The results confirm previous observations that suggested fibrous root loss as one of the major consequences of infection and colonization with *C*Las. They also reinforce the benefits of using IPCs to prevent infection of young citrus trees during the first years of growth in the field.**

Huanglongbing (HLB), or citrus greening, is associated with a phloem-limited bacterial pathogen that causes extensive systemic damage to citrus trees that results in low yields, poor fruit quality, and whole tree decline (Bové 2006; da Graça et al. 2015; Gottwald et al. 2007). In Florida, the disease is associated with the putative pathogen *Candidatus* Liberibacter asiaticus (*C*Las) and transmitted by the Asian citrus psyllid (*Diaphorini citri*) (Halbert 2005; Halbert and Manjunath, 2004). Currently, HLB is the most significant threat to the global citrus industry and has already drastically reduced production in Florida, where it is now considered endemic (Graham et al. 2020). Although research of HLB has been extensive since the pathogen was first detected in the Americas (Gottwald et al. 2007), the understanding of the movement and distribution of *C*Las after infection is limited. Studies have found that *C*Las can colonize the roots before the leaves, where they replicate and move back to the leaves when new flushes become sinks and phloem movement is reversed (Johnson et al. 2014). It was also suggested that fibrous root decline is a primary consequence of *C*Las infection and can be seen before the occurrence of symptoms in aboveground tissue (Graham et al. 2013; Johnson et al. 2014). However, root colonization by *C*Las is generally lower than colonization in aboveground tissue (Braswell et al. 2020; Tardivo et al. 2023) and may be rootstock-dependent (Bodaghi et al. 2022a, 2022b; Bowman and Albrecht 2020).

Despite the pervasiveness of the bacteria and the damage it has caused the citrus industry, *C*Las has not yet been isolated in pure culture and is difficult to maintain in a controlled environment. This has hampered research because of the challenge of uniformly infecting trees in a greenhouse setting (Bodaghi et al. 2022a, 2022b; Bowman and Albrecht 2020). Moreover, greenhouse-grown trees that are infected using graft or psyllid inoculation often have lower levels of bacteria and fewer disease symptoms than trees exposed to natural conditions, which may be attributed to the one-time inoculation typically received in the greenhouse compared with the constant reinoculation by psyllids in the field. *C*Las-induced growth reductions of trees confined to a container, especially of the roots, may not truly reflect the reductions that occur under open field conditions. Because of the endemic nature of the disease in Florida, it is difficult to establish experiments that compare infected trees with noninfected trees in a field setting.

Conventional HLB management practices, such as soil drenches and foliar sprays of insecticides, have been ineffective at adequately controlling the psyllids. One technique that growers have begun implementing for psyllid management in young trees is the use of individual protective covers (IPCs). The IPC is used to exclude vectors and can effectively prevent infection with *C*Las in HLB-endemic conditions (Alferez et al. 2021; Gaire et al. 2022). The environment inside the IPCs also has several effects on the physiology of the trees. Specifically, the shading and reduced vapor pressure deficit underneath the IPCs promote photosynthesis, resulting in more vegetative growth and overall improved tree health (Gaire et al. 2022; Vincent et al. 2023). IPCs also protect against leaf miners and citrus canker, but they may create an environment more conducive to colonization with other pests and certain fungal pathogens such as sooty mold (Gaire et al. 2022). Additionally, the use of IPCs will physically restrict canopy expansion, causing bending and twisting of branches; however, the long-term effects are still being investigated. Despite the costs and challenges associated with IPC use, many growers across Florida have begun implementing this technology as part of their HLB management program.

In this study, IPCs were used as a strategy to compare field-grown infected and noninfected 'Valencia' trees on two different rootstocks with similar morphological and physiological traits in an HLB-endemic environment. The objectives were to monitor the distribution and accumulation of *C*Las in the aboveground and belowground tissues following psyllid colonization, identify differences

in aboveground and belowground physiological effects, and understand the extent of growth reductions, especially of the root system, during the early phase of growth.

Materials and Methods

Plant material

The trees used in this study were 'Valencia' sweet orange (*Citrus sinensis*) grafted on US-812 (*C. reticulata* 'Sunki' × *Poncirus trifoliata* 'Benecke') and US-942 (*C. reticulata* 'Sunki' × *P. trifoliata* 'Flying Dragon') rootstock. Both rootstocks are considered HLB-tolerant, whereas 'Valencia' orange is considered HLB-susceptible (Albrecht and Bowman, 2019). Plants were grown in a controlled disease-free greenhouse at the Southwest Florida Research and Education Center (SWFREC) in Immokalee (Collier County), FL, USA. Two-year old trees were planted in December 2020 in two rows on a raised bed at the SWFREC research farm (26.463663 °N, 81.443892 °W). Between-row and within-row spacings were 22 feet (6.7 m) and 8 feet (2.44 m), respectively. Trees were fertilized at a rate of 0.5 pounds (0.23 kg) per tree using conventional granular fertilizer (8N–4P–8K; Diamond R, Fort Pierce, FL, USA) every 6 months and slow-release fertilizer (12N–8P–6K; Diamond R) once per year. Irrigation was performed by under-tree microjets. No insecticides were applied, and psyllid populations were consistently high during periods of new vegetative flush throughout the year.

Experimental design

The trial was arranged in a completely randomized 2 × 2 factorial design with seven replications, with each consisting of linear plots of two trees. The first factor (disease state) had two levels: noninfected and infected. The second factor (rootstock) had two levels: US-812 and US-942.

To create healthy trees, IPCs (Tree Defender Inc., Dundee, FL, USA) were installed on half of the trees immediately upon transplanting into the field. The IPCs had a height of 6 feet (1.2 m) and were made of monofilament high-density polyethylene with a mesh size of 50. A PVC pole was installed next to each tree for support, and IPCs were tied at the base of the trunk. To create infected trees, the other half of the trees were covered with IPCs in the same manner, but four 15- × 15-cm openings were cut into the mesh of the IPCs to allow for psyllid infestation ("open IPCs") (Fig. 1). Covering all trees ensured that any physiological and morphological effects induced by the IPCs were the same for both treatments. To promote infection, in both 2021 and 2022, the open IPCs were fully removed at the beginning of the main flushing period (February–March) and replaced when most flush had fully hardened (after ~6 weeks).

Fig. 1. Photograph obtained in Jun 2022. Individual protective covers (IPCs) with 15- × 15-cm openings (arrow) were used to preserve consistency and equalize the physiological and morphological effects associated with IPCs.

*C*Las detection

Leaves and fibrous roots were collected every 2 months starting in Apr 2021. Two leaves were randomly collected from different areas in the canopy from each replicate tree and pooled. Leaves were collected from the most recent mature flush and stored at −20 °C until analysis. Fibrous roots (<2 mm in diameter) were collected by gently digging into the top 10 cm of the soil underneath the canopy drip line. Roots were pooled within replications, washed, blotted dry, and stored at −20 °C until analysis. A 4-mm-diameter round section was cut from the midvein of each leaf directly adjacent to the leaf petiole using a hole puncher. Four leaf punches were pulverized by freezing with liquid nitrogen and shaking for 90 s in a BioSpec Mini-Beadbeater-96 (Bartlesville, OK, USA). Fibrous roots were pulverized with liquid nitrogen using a mortar and pestle. Then, 100 mg of tissue was used for DNA extraction using the DNeasy Plant Pro Kit (Qiagen, Valencia, CA, USA) according to the manufacturer's instructions. Real-time polymerase chain reaction assays were performed using primers HLBas/HLBr and probe HLBp (Li et al. 2006). Primers COXf/COXr and probe COXp (Li et al. 2006) were used for internal control and normalization. Previous studies showed that these primers are suitable for both leaf and root detection of *C*Las (Tardivo et al. 2023). Amplifications were performed using an Applied Biosystems QuantStudio 3 Real-Time polymerase chain reaction system (Applied Biosystems, Foster City, CA, USA) and the iTaq Universal Probes Supermix (Bio-Rad, Hercules, CA, USA) according to the manufacturer's instructions. All reactions were performed in a 20-µL reaction volume using 2 µL DNA. If no signal was detected after 40 cycles of amplification, then a cycle threshold (Ct) value of 41 was assigned for statistical purposes.

Root growth analysis

To measure root growth over time, 6- × 50-cm clear acrylic minirhizotron tubes (CID BioScience, Camas, WA, USA) were inserted next to each tree at planting. The tubes were installed 20 cm from the tree trunk and perpendicular to the soil surface. Each tube was closed at the bottom and capped at the top to prevent light and water from entering. Beginning in Jul 2021, root images were captured every other month using a CI-600 in situ root imaging system (CID Bio-Science). Each 30.5- × 20.0-cm image represented a 360-degree view of the root zone growing along the surface of the tube. Root images were analyzed using RootSnap software (CID-Bioscience Ltd., Camas, WA, USA). Live root growth was measured as the total length of live roots visible in the imaging area and expressed in millimeters; live and dead roots were distinguished by their color and structural integrity. Root growth was measured for 1 year; during that time, there was no overlap of roots from adjacent trees.

Leaf and fibrous root enzymatic carbohydrate analysis

In Oct 2021, Feb 2022, and Jun 2022, the nonstructural carbohydrate contents of leaves and roots was determined for the same tissue samples collected for *C*Las analysis. The soluble (sugars and sugar alcohols) and insoluble (starch) carbohydrate contents were measured following the enzymatic protocol described by Leyva et al. (2008) with modifications described by Tixier et al. (2017) and Davidson et al. (2021).

Tree trunk size and canopy health

Measurements were conducted 18 months after planting. Scion and rootstock trunk diameters were measured at 5 cm above and below the graft union. Visual ratings of tree health included canopy color and foliar HLB disease symptoms. Canopy color was rated using a scale of 1 to 5 (1 = very yellow and 5 = dark green). The HLB disease symptom severity was rated using a scale of 1 to 5 (1 = 0% of branches with HLB symptoms; 2 = 0%–25% of branches with HLB symptoms; 3 = 25%–50% of branches with HLB symptoms; 4 = 50%–75% of branches with HLB symptoms; 5 = >75% of branches with HLB symptoms). The HLB disease symptoms were defined as irregular blotchy mottling of the leaves typical for HLB (Gottwald et al. 2007).

Leaf nutrients, leaf size, and leaf relative water content

Leaf nutrients were analyzed in Jul 2022 using 30 randomly collected mature leaves per replication from the most recent spring flush. An analysis of macronutrients (nitrogen,

Received for publication 18 Dec 2023. Accepted for publication 31 Jan 2024.
Published online 26 Mar 2024.
C.T. and L.A. contributed equally to this work.
This research was supported by grants from the Citrus Research and Development Foundation (CRDF), US Department of Agriculture (USDA) National Institute of Food and Agriculture (NIFA) Specialty Crop Research Initiative (SCRI) project 2022-70029-38481, and USDA NIFA Hatch project FLA-SWF-006160.
We thank the Plant Physiology laboratory team for their excellent laboratory and field assistance.
U.A. is the corresponding author. E-mail: ualbrecht@ufl.edu.

Table 1. Cycle threshold (Ct) values of leaves and roots of exposed (infected) 'Valencia' trees grafted on two rootstocks from Apr 2021 to Jul 2022.

	Apr 2021	Jun 2021	Aug 2021	Oct 2021	Dec 2021	Feb 2022	Apr 2022	Jul 2022
Tissue								
Leaves	36.7 b	37.6	36.7	31.2	31.3	27.2 b	27.3	31.1 b
Roots	40.0 a	34.5	37.1	30.4	31.0	35.2 a	28.8	38.1 a
P value	0.017	0.102	0.820	0.784	0.929	0.006	0.546	<0.0001
Rootstock								
US-812	39.0	37.7	39.4 a	34.7 a	33.7	33.8	31.1 a	34.9
US-942	37.9	34.4	34.4 b	26.8 b	28.5	28.6	24.9 b	34.2
P value	0.327	0.087	0.021	0.019	0.121	0.063	0.021	0.553
Tissue × rootstock								
P value	0.435	0.976	0.992	0.896	0.613	0.705	0.163	0.341

Different letters within columns indicate significant differences ($P < 0.05$) according to Tukey's honestly significant difference test.

phosphorus, potassium, calcium, magnesium, sulfur) and micronutrients (boron, zinc, manganese, iron, copper) was conducted by Waters Agricultural Laboratories, Inc. (Camilla, GA, USA). The total nitrogen content was determined by the combustion method described by Sweeney (1989). The other macronutrients and micronutrients were analyzed using inductively coupled argon plasma atomic emission spectroscopy after digesting leaves with nitric acid and hydrogen peroxide (Huang and Schulte 1985).

The average leaf size was determined by scanning 20 randomly selected leaves per tree at 400 dpi on a flatbed scanner (Epson Perfection v850 Pro; Epson America, Los Alamitos, CA, USA) and calculating the leaf area using Fiji software (Schindelin et al. 2012). The leaf relative water content was measured from five leaves per tree using the newest hardened-off leaves with no damage. The relative water content was calculated following the protocol established by Lugojan and Ciulca (2011).

Table 2. Live root growth of noninfected and infected 'Valencia' trees grafted on two rootstocks from Jul 2021 until Jul 2022.

	Live root length (mm)
Disease state	
Noninfected	21.7 a
Infected	17.3 b
P value	0.041
Rootstock	
US-812	21.0
US-942	17.9
P value	0.167
Time	
Jul 2021	9.3 b
Sep 2021	17.5 ab
Nov 2021	19.9 ab
Jan 2022	20.0 ab
Mar 2022	22.8 a
May 2022	23.0 a
Jul 2022	23.9 a
P value	0.004
Disease state × rootstock	
P value	0.230
Disease state × time	
P value	0.735
Rootstock cultivar × time	
P value	1.000
Disease state × rootstock × time	
P value	0.454

Different letters within columns indicate significant differences ($P < 0.05$) according to Tukey's honestly significant difference test.

Stomatal conductance

Before excavation, stomatal conductance was measured on three leaves per tree between 9:00 AM and 11:00 AM using an SC-1 leaf porometer (METER Group, Pullman, WA, USA) following the manufacturer's guidelines. Leaves were chosen from the newest hardened-off flush in direct sunlight with no insect damage and minimal symptoms of HLB or nutritional deficiencies. The porometer was calibrated in the field on the day of the excavation, and measurements were taken using the "Auto" mode on the abaxial side of each leaf, avoiding the midrib or large leaf veins.

Tree excavation and biomass distribution

In Jul 2022, a subset of 16 trees (four trees per experimental unit) was excavated to measure aboveground and belowground biomasses and root size distribution. Excavations were completed using a pneumatic arborist tool (2000 Model HT142; Airspade, Chicopee, MA, USA) connected to a compressed air tank that allowed the removal of the whole root system with minimal damage or loss of fibrous roots. Each tree was cut at the soil surface to separate aboveground and belowground tissues. The excavated root systems were washed and separated into fibrous roots (<2 mm in diameter), nonfibrous roots, and root crowns. All tissue were dried at 60 °C to determine dry weights.

Specific root length and root respiration

To determine the specific root length, a subset of fibrous roots from each excavated tree was scanned on a flatbed scanner (Epson Perfection V850) at 400 dpi. The root length was measured using Assess 2.0 (Lamari, 2008), and the specific root length was calculated by dividing the fibrous root length (m) by the dry weight (g). Root respiration of another subset of fibrous roots was measured following the protocol of Bodaghi et al. (2022b). Measurements were conducted in a closed-loop 50-mL respiration chamber using a LI-850 CO_2/H_2O analyzer (LICOR, Lincoln, NE, USA) over a 5-minute interval. Then, the root tissue was dried at 60 °C and weighed to express respiration rates relative to their dry mass.

Trunk and pioneer root starch content using iodine staining

Excavated trees were cut crosswise using a band saw (Micromark, Berkeley Heights, NJ, USA) to create 1-cm-thick sections of pioneer roots (5–6 mm in diameter), rootstock trunk (5 cm below the graft union), lower scion trunk (5 cm above the graft union), and upper scion trunk (directly below the lowest scaffold branch). Three adjacent disks were cut from each tissue for three technical replicates per tissue type and tree. The starch content of these tissue sections was measured using the iodine staining technique described by Etxeberria et al. (2009). Briefly, tissue was submerged in a 10% iodine tincture solution for 2 min, rinsed, and immediately scanned at 600 DPI on a flatbed scanner (Epson Perfection v850 Pro). The stained area of each section, which indicated the presence of starch, was calculated using

Table 3. Leaf and root soluble sugar and starch contents of noninfected and infected 'Valencia' trees grafted on two rootstocks.

	Soluble sugars (μg/mg tissue)			Starch (μg/mg tissue)		
	21 Oct	22 Feb	22 Jun	21 Oct	22 Feb	22 Jun
Disease state						
Noninfected	51.3	75.2	91.8	70.6	17.5 b	30.7
Infected	59.4	73.6	95.7	67.6	29.1 a	36.0
P value	0.261	0.731	0.446	0.913	0.005	0.193
Tissue						
Leaves	59.1	101.3 a	111.6 a	103.9 a	25.9	57.0 a
Roots	51.6	47.5 b	75.9 b	34.3 b	20.7	9.6 b
P value	0.298	<0.0001	<0.0001	<0.0001	0.20	<0.0001
Rootstock						
US-812	111.0	96.5	98.0	57.0	22.5	32.8
US-942	136.0	98.8	105.0	79.3	24.1	38.0
P value	0.052	0.768	0.497	0.087	0.699	0.45
Disease state × rootstock						
P value	0.233	0.774	0.520	0.177	0.860	0.542
Disease state × tissue						
P value	0.655	0.275	0.054	0.402	0.475	0.284

Different letters within columns indicate significant differences ($P < 0.05$) according to Tukey's honestly significant difference test.

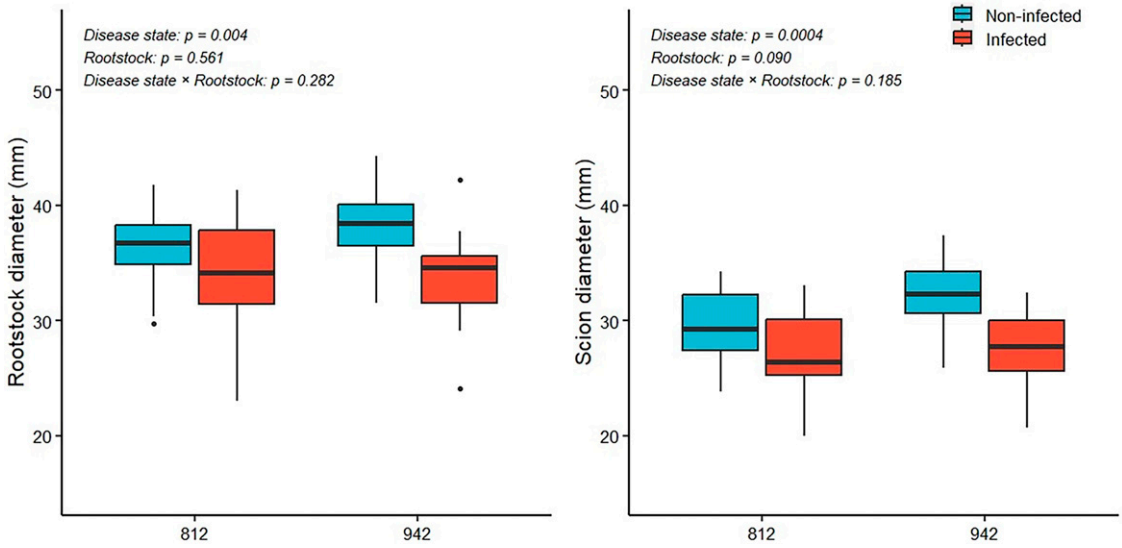

Fig. 2. Trunk size of noninfected and infected 'Valencia' trees on two rootstocks after 18 months of field growth.

ImageJ 1.52p software by converting images to grayscale and using a global threshold for all images.

Statistical analysis

All analyses were conducted using R version 4.0.3 (R Core Team 2021).

Analysis of variance. Before the analysis of variance (ANOVA), data were tested for the assumptions of normality and homogeneity of variance. Comparisons of the bacterial titer were performed using a two-way repeated-measures ANOVA with rootstock and tissue type as factors. The carbohydrate content was compared at each time point using an additive three-way ANOVA with rootstock, disease state, and tissue type as factors. Tree growth measurements and leaf and root analyses were analyzed using a two-way ANOVA with rootstock and disease state as factors. Tree biomass distribution, root respiration, and stomatal conductance measurements were analyzed from four single-tree replications; all other measurements were analyzed from all seven two-tree replications. When differences were significant ($P < 0.05$), a post hoc comparison of means was calculated using Tukey's honest significant difference test. Visual ratings of tree health were analyzed nonparametrically using an aligned ranks transformation ANOVA.

Principal component analysis. The principal component analysis (PCA) of the standardized data was performed to reduce the effects of different measurement scales among variables (Sneath and Sokal 1973). The PCA was performed using the FactoMine R package in R 4.0.3 (Lê et al. 2008). The PCA was divided between aboveground and belowground measurements to account for data variability. Above ground factors included total aboveground biomass (TAMASS), scion trunk diameter (STDIA), leaf Ct (LFCT) values, canopy color (CCOLOR), leaf size (LFSIZE), HLB symptoms (HLBSYM), and leaf starch content (LFSTARCH). Belowground factors included total belowground biomass (TBMASS), rootstock trunk diameter (RTDIA), fibrous root mass (FIBR), nonfibrous root mass (NONFIBR), root crown mass (RCROWN), fibrous root Ct (FIBRCT) values, and fibrous root starch content (FIBRSTARCH).

Results

CLas detection

*C*Las titers are expressed as the Ct value; high Ct values indicate a low *C*Las titer, and low Ct values indicate a high *C*Las titer. No amplification signal was detected in samples from trees that remained covered with the IPCs throughout the trial (data not shown), thus confirming that trees were not infected and that there was no cross-contamination with other organisms (Shin and van Bruggen 2018). In trees that were exposed to psyllids, *C*Las was

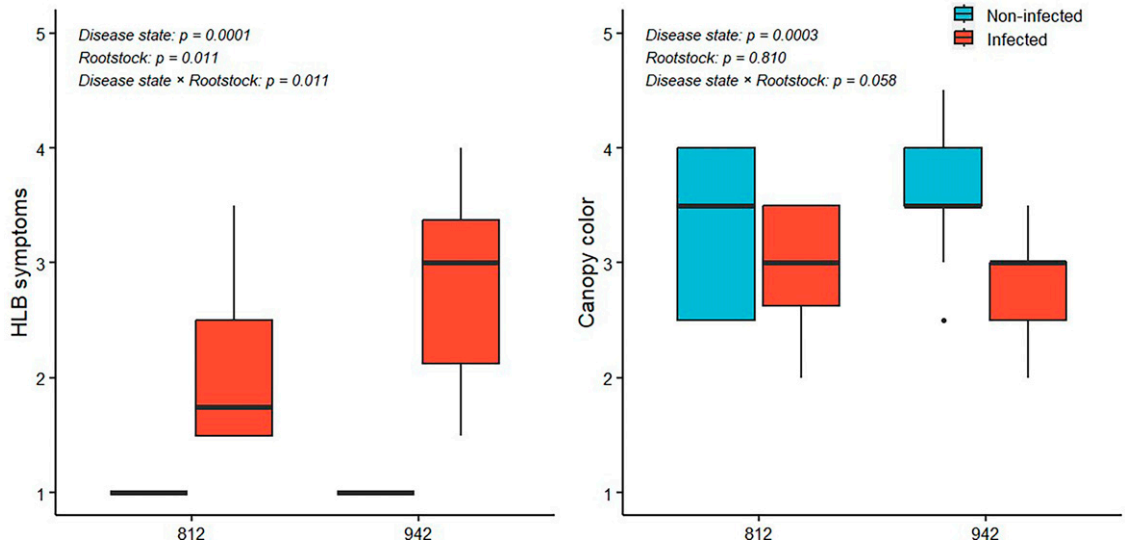

Fig. 3. Canopy health of noninfected and infected 'Valencia' trees on two rootstocks after 18 months of field growth. Huanglongbing (HLB) symptoms are expressed using a scale of 1 to 5 (1 is the best and 5 is the worst). Canopy color is expressed using a scale of 1 to 5 (1 is the worst and 5 is the best).

Table 4. Leaf size and relative water content of noninfected and infected 'Valencia' trees on two rootstocks after 18 months of field growth.

	Leaf size (cm^2)	Leaf relative water content (%)
Disease state		
Noninfected	39.6 a	92.6
Infected	25.2 b	91.5
P value	<0.0001	0.055
Rootstock		
US-812	32.1	91.5
US-942	32.7	92.6
P value	0.738	0.053
Disease state × rootstock		
P value	0.059	0.430

Different letters within columns indicate significant differences ($P < 0.05$) according to Tukey's honestly significant difference test.

detected as early as Apr 2021 (4 months after planting). In Apr 2021, Feb 2022, and Jul 2022, the Ct values of the roots were significantly higher than the Ct values of the leaves, indicating higher bacterial titers in the leaves than in the roots (Table 1). In Aug and Oct 2021 and Apr 2022, the Ct values were higher for trees on US-812 than US-942. The lowest leaf Ct values (highest bacterial titers) were measured in Feb and Apr 2022. The lowest root Ct values were measured in Apr 2022.

Root growth

The average live root length of infected trees was 25% less (17.3 mm) than that of noninfected trees (21.7 mm) (Table 2). No significant differences between rootstocks were observed. There was an increase in the live root length over time across both cultivars and disease states; significantly more roots were measured in Mar, May, and Jul 2022 than in Jul 2021. There were no significant interaction effects between disease state, rootstock, and time.

Leaf and fibrous root enzymatic carbohydrate content

Soluble sugars. The soluble sugar content did not differ significantly between healthy and infected trees (Table 3). In Feb and Jun 2022, the leaf soluble sugar content was significantly higher (101.3 and 111.6 μg/mg, respectively) than the root soluble sugar content (47.5 and 75.9 μg/mg, respectively). There was no significant interaction between disease state and tissue or rootstock.

Starch. In Feb 2022, there was significantly more starch in the infected trees (29.1 μg/mg) than in the noninfected trees (17.5 μg/mg) (Table 3). This effect was not measured during the other months. In Oct 2021 and Jun 2022, the leaf starch content was significantly higher (103.9 and 57.0 μg/mg, respectively) than the root starch content (34.3 and 9.6 μg/mg, respectively). There was no significant difference between rootstocks, nor was there a significant interaction between disease state and tissue or rootstock.

Tree growth and health

In Jun 2022, 18 months after field planting, there were significant differences in the trunk size between noninfected and infected trees (Fig. 2). The scion and rootstock trunk diameters of infected trees averaged for both rootstocks were significantly smaller (27.3 mm and 34.1 mm, respectively) than those of noninfected trees (30.7 mm and 37.4 mm, respectively). There were no significant differences among rootstocks, nor were there any interactions.

Noninfected trees were healthy, with no HLB symptoms, and had a greener canopy than the infected trees (Fig. 3). Among the infected trees, those on US-942 had significantly more visual symptoms of HLB than those on US-812 (Fig. 3).

Leaf size, leaf relative water content, and leaf nutrient content

The leaf size of infected trees was significantly smaller (25.2 cm^2) than the leaf size of noninfected trees (39.6 cm^2) (Table 4). There was a trend for the leaf relative water content to be higher in healthy trees than in infected trees ($P = 0.055$) and to be higher in combination with US-942 than US-812 ($P = 0.053$), but the differences were small.

Infected trees contained less potassium, calcium, and magnesium than noninfected trees (Table 5). Trees on US-942 had more leaf nitrogen and less magnesium than trees on US-812. Infected trees on US-942 had the lowest leaf calcium levels of all trees.

Leaf micronutrient contents were higher in infected than in noninfected trees except for zinc (Table 6). Trees on US-812 had a higher leaf boron content (111.0 ppm) than trees on US-942 (103.0 ppm), but there were no other significant rootstock effects.

Biomass distribution

Biomasses were measured on the excavated subset of trees. The aboveground biomass was 20% smaller in infected trees than in noninfected trees (Table 7, Fig. 4) but there was a significant interaction with the rootstock. The aboveground biomass was larger for noninfected trees on US-942 (1532 g) than for infected trees on US-942 (960 g), but neither was significantly different from trees on US-812. The total belowground biomass was reduced from 668 g in noninfected trees to 422 g in infected trees (37% reduction). The fibrous root and nonfibrous root biomasses were significantly reduced from 104 g and

Table 5. Leaf macronutrients of noninfected and infected 'Valencia' trees on two rootstocks after 18 months of field growth.

	N (%)	P (%)	K (%)	Ca (%)	Mg (%)	S (%)
Disease state						
Noninfected	2.79	0.20	1.88 a	4.04 a	0.39 a	0.30
Infected	2.89	0.19	1.70 b	3.67 b	0.34 b	0.29
P value	0.127	0.306	0.0002	0.002	<0.0001	0.523
Rootstock						
US-812	2.77 b	0.20	1.81	3.93	0.39 a	0.30
US-942	2.91 a	0.19	1.77	3.78	0.34 b	0.30
P value	0.027	0.926	0.420	0.183	<0.0001	0.855
Disease state × rootstock						
Noninfected × US-812	2.73	0.21 a	1.90	3.95 a	0.41	0.29 a
Infected × US-812	2.80	0.18 a	1.72	3.91 a	0.37	0.31 a
Noninfected × US-942	2.85	0.19 a	1.87	4.13 a	0.37	0.31 a
Infected × US-942	2.97	0.20 a	1.68	3.43 b	0.31	0.28 a
P value	0.674	0.044	0.831	0.005	0.209	0.005

Different letters within columns indicate significant differences ($P < 0.05$) according to Tukey's honestly significant difference test.
Ca = calcium; K = potassium; Mg = magnesium; N = nitrogen; P = phosphorus; S = sulfur.

Table 6. Leaf micronutrients of noninfected and infected 'Valencia' trees on two rootstocks after 18 months of field growth.

	B (ppm)	Zn (ppm)	Mn (ppm)	Fe (ppm)	Cu (ppm)
Disease state					
Noninfected	102.0 b	22.4	30.9 b	101.0 b	10.8 b
Infected	111.0 a	22.0	39.5 a	123.0 a	14.3 a
P value	0.020	0.767	0.0001	0.015	<0.0001
Rootstock					
US-812	111.0 a	21.9	34.9	117.0	13.2
US-942	103.0 b	22.4	35.5	108.0	12.0
P value	0.035	0.678	0.770	0.305	0.052
Disease state × rootstock					
Noninfected × US-812	103.0	20.8 a	31.6	105.7	11.6
Infected × US-812	118.0	23.1 a	38.2	128.0	14.7
Noninfected × US-942	102.0	23.9 a	30.1	96.3	10.0
Infected × US-942	104.0	20.9 a	40.9	118.9	13.9
P value	0.097	0.032	0.329	0.984	0.486

Different letters within columns indicate significant differences ($P < 0.05$) according to Tukey's honestly significant difference test.
B = boron; Cu = copper; Fe = iron; Mn = manganese; Zn = zinc.

Table 7. Biomass of aboveground and belowground tissues of noninfected and infected 'Valencia' trees on two rootstocks after 18 months of field growth.

	Aboveground tissue (g)	Belowground tissue (g)	Fibrous roots (g)	Nonfibrous roots (g)	Root crown (g)
Disease state					
Noninfected	1436 a	668 a	104 a	234 a	330 a
Infected	1156 b	422 b	53 b	139 b	230 b
P value	0.024	0.0007	0.001	0.001	0.004
Rootstock					
US-812	1346	560	81	201	279
US-942	1246	530	76	172	281
P value	0.379	0.583	0.720	0.221	0.940
Disease state × rootstock					
Noninfected × US-812	1340 ab	626	98	236	292 ab
Infected × US-812	1351 ab	495	64	165	266 ab
Noninfected × US-942	1532 a	711	111	232	368 a
Infected × US-942	960 b	348	42	112	194 b
P value	0.020	0.056	0.168	0.298	0.020

Tree biomass distribution was analyzed from four single-tree replications (trees that were excavated). Different letters within columns indicate significant differences ($P < 0.05$) according to Tukey's honestly significant difference test.

224 g, respectively, in noninfected trees to 234 g and 139 g, respectively, in infected trees (Table 7, Fig. 5) (reductions of 49% and 40%). The dry weight of the root crown was larger for noninfected US-942 than for infected US-942, but neither was significantly different from US-812.

The ratio of the belowground to the aboveground dry biomass was significantly smaller for infected trees compared with noninfected trees, and there was no significant rootstock effect or interaction (Fig. 6); average ratios across both rootstocks were 0.36 (infected trees) and 0.47 (noninfected trees). The ratio of the fibrous root dry biomass to the whole root dry mass was also smaller in infected trees than in noninfected trees, with no significant rootstock effect or interaction (Fig. 6). The average ratios across both rootstocks were 0.14 (infected trees) and 0.18 (noninfected trees). A similar reduction for the ratio of the fibrous roots to the aboveground biomass was measured.

Fig. 4. Effect of *Candidatus* Liberibacter asiaticus infection on aboveground biomass 18 months after field planting.

Fig. 5. Effect of *Candidatus* Liberibacter asiaticus infection on belowground biomass 18 months after field planting.

Trunk and pioneer root starch content using iodine staining

All variables of the excavated subset of trees were measured. There was no significant difference in the starch contents of the upper and lower scion trunks and pioneer roots of noninfected and infected trees (Table 8, Supplemental Fig. 1). In the rootstock trunk, more than twice as much starch was measured in infected trees than in noninfected trees. US-942 accumulated significantly more starch in the rootstock trunk than US-812, but there were no significant rootstock effects for the upper and lower scion trunks. A significant interaction was found for the pioneer roots. Noninfected US-942 pioneer roots accumulated the most starch, whereas healthy US-812 roots accumulated the least.

Specific root length, root respiration, and stomatal conductance

All variables of the excavated subset of trees were measured. There were no significant differences in the specific root length, root respiration rate, and stomatal conductance between infected and noninfected trees and between rootstocks, nor were there any interaction effects (Supplemental Fig. 1).

Principal component analysis

A PCA was conducted to assess the relationship between disease state and rootstock. For aboveground variables, healthy and infected trees were separated along principal component 1, which explained 80.4% of the variance (Fig. 7). Separation was most strongly influenced by the leaf bacterial titer (Ct values), total aboveground biomass, scion trunk diameter, and HLB symptoms.

For belowground measurements, healthy and infected trees were also separated along principal component 1, which explained 76.4% of the variance (Fig. 8). The separation in dimension 1 was driven mostly by the total root biomass, fibrous root biomass, and fibrous root Ct value.

Discussion

In trees that had been exposed to psyllids, *C*Las was first detected in April, soon after the major flushing period. This is consistent with the findings of Hall et al. (2016), who demonstrated that the presence of new flush attracts psyllids and increases the probability of infection. Infection levels were low at that time, and Ct values were lower in the leaves than in the roots, indicating a greater bacterial load in the former. This pattern was also observed in Feb 2022, and at the time of tree excavation in Jul 2022, which is in accordance with previous studies that demonstrated that Ct-values are generally higher, and therefore bacterial titers lower, in the roots than in the leaves (Bowman and Albrecht 2020; Tardivo et al. 2023). Johnson et al. 2014 suggested that *C*Las colonizes the roots first; however, this was not found in this study. In contrast to our study, inoculations in that study were performed by budding, and plants were maintained

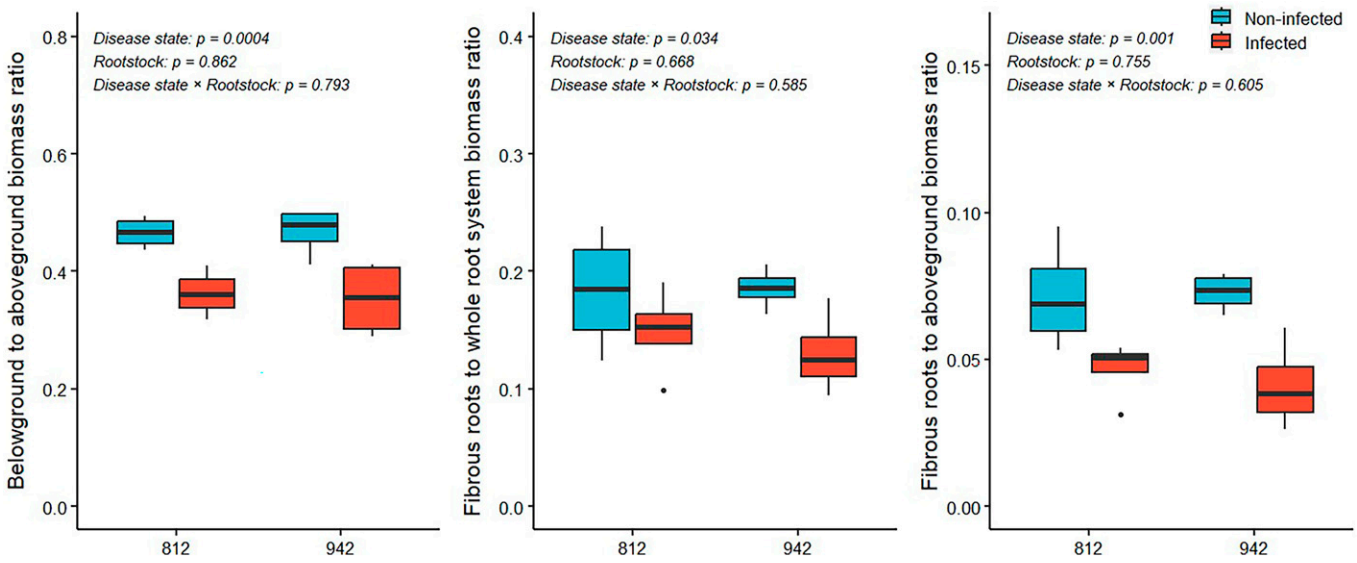

Fig. 6. Biomass ratios of noninfected and infected 'Valencia' trees on two rootstocks after 18 months of field growth.

in controlled greenhouse conditions. Our findings are also different from those of Tardivo et al. (2023), who detected *C*Las first in the fibrous roots of young citrus trees after natural psyllid inoculation. Differences in source–sink relationships at the time of infection likely contributed to the different results. In this study, trees were planted in December, and root systems were established by the time the trees were most heavily exposed to psyllids. In the study by Tardivo et al. (2023), trees were exposed to psyllids in spring, immediately after planting, thus promoting *C*Las movement to the roots, which were likely a strong sink for photosynthates at that time. *C*Las moves rapidly and most predominantly toward new tissue growth, as demonstrated by Raiol-Junior et al. (2021).

Phloem collapse and metabolic abnormalities caused by HLB cause starch accumulation in the leaves (Albrecht and Bowman 2008; Brodersen et al. 2014; Etxeberria et al. 2009; Fan et al. 2010). Except for Feb 2022, we did not find significant leaf starch accumulations in infected trees. Contrary to the findings of other studies (Achor et al. 2010; Aritua et al. 2013; Etxeberria et al. 2009; Kim et al. 2009), there was no indication of carbohydrate depletion in the roots in response to infection. During a greenhouse experiment, Kumar et al. (2018) found that HLB-induced root decline and starch depletion varied based on the root order. The authors found that higher-order roots were most deprived in photosynthates, thus promoting the decline of lower-order roots that were not deprived. The lack of starch deprivation in the fibrous roots found in this study is in line with those findings. Using iodine staining, we found less starch in the higher-order (pioneer) roots of infected rather than noninfected US-942. This was not observed for US-812, suggesting that HLB had progressed less in this rootstock than in US-942. Contrary to the pioneer roots, we observed more starch accumulation in the rootstock portion of infected trees and in US-942. No differences were found in the upper and lower scions, suggesting that the rootstock plays a role in the source–sink relationships of grafted trees.

Table 8. Starch contents of trunk and pioneer roots of noninfected and infected 'Valencia' trees grafted on two rootstocks measured by iodine staining.

	Upper scion trunk (%)	Lower scion trunk (%)	Rootstock trunk (%)	Pioneer roots (%)
Disease state				
Noninfected	31.2	31.7	6.3 b	29.6
Infected	48.7	31.5	13.3 a	24.8
P value	0.155	0.985	0.007	0.224
Rootstock				
US-812	41.3	33.2	6.5 b	23.2
US-942	38.5	30.0	13.1 a	31.2
P value	0.815	0.838	0.010	0.055
Disease state × rootstock				
Noninfected × US-812	33.5	39.0	4.0	21.0 b
Infected × US-812	49.1	27.4	9.0	25.4 ab
Noninfected × US-942	28.8	24.0	8.6	38.2 a
Infected × US-942	48.3	35.5	17.6	24.2 ab
P value	0.871	0.464	0.366	0.031

Upper scion disks were collected from 0 to 5 cm below the lowest scaffold. Lower scion disks were collected from 5 to 10 cm above the graft union. Rootstock disks were collected from 5 to 10 cm below the graft union. Roots measuring 5 to 6 mm in diameter were collected. Different letters within columns indicate significant differences ($P < 0.05$) according to Tukey's honestly significant difference test.

Protecting trees with screens such as IPCs increases the humidity, reduces the vapor pressure deficit, and lowers the air temperature within the screen (Alarcón et al. 2006; Budiarto et al. 2019; Gaire et al. 2022; Mahmood et al. 2018). This has been tied to higher rates of photosynthesis, stomatal conductance, CO_2 assimilation, and water use efficiency (Budiarto et al. 2019; Pegoraro et al. 2005; Syvertsen and Levy 2005). All trees in this study were covered with IPCs to maintain similar environmental and physical conditions between healthy and infected trees. This hindered canopy expansion and prevented our ability to clearly measure changes in tree height and canopy volume between infected and noninfected trees. However, the canopy volume of infected trees was visibly smaller compared with that of noninfected trees (Fig. 5). Within the first year after infection, the rootstock and scion trunk diameters and the leaf size of infected trees were significantly smaller than those of noninfected trees, suggesting that phloem collapse and resulting metabolic disturbances typically associated with HLB manifest quickly in young trees growing in HLB-endemic conditions. Leaf size reductions are one of the most predictive effects of HLB severity, even in the absence of other foliar symptoms (Bodaghi et al. 2022a; Bowman and Albrecht 2020; Yu et al. 2023).

Leaves from both noninfected and infected trees had optimal concentrations of most macronutrients except potassium and magnesium, which were below optimum levels in infected trees (Morgan and Kadyampakeni 2020). As observed during a recent greenhouse study (Bodaghi et al. 2022a), infected trees also had significantly less calcium than noninfected trees. Leaf micronutrients for both infected and noninfected trees were in the optimum range, except for zinc, which was below the optimal range regardless of the disease state. Despite being within the recommended range, leaves of infected trees had significantly more

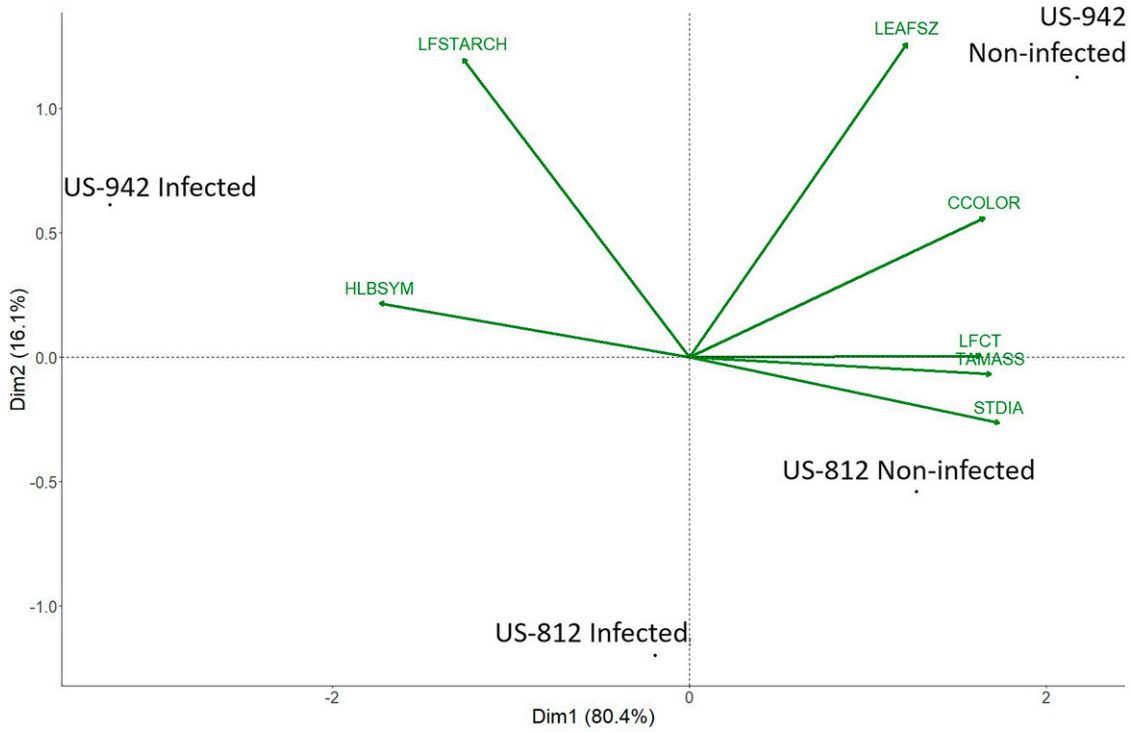

Fig. 7. Principal component analysis biplot of significant aboveground variables. CCOLOR = canopy color; Dim1 = dimension 1; Dim2 = dimension 2; HLBSYM = Huanglongbing symptoms; LEAFSZ = leaf size; LFCT = leaf cycle threshold value; LFSTARCH = leaf starch content; STDIA = scion trunk diameter; TAMASS = total aboveground biomass.

leaf micronutrients than noninfected trees. This is consistent with results of Gaire et al. (2023) regarding the levels of copper, manganese, and boron in a grove with similar management. In the absence of foliar sprays that could have easily penetrated the holes of IPCs, the reason for these differences in micronutrient contents in two independent studies remains unclear and warrants further investigation.

Although comparable to US-812 for many traits, US-942 has been the most popular rootstock in Florida since 2018 (Rosson 2022), and it performs well in the presence of HLB (Albrecht and Bowman 2012; Bowman et al. 2016a, 2016b). During this study, trees with US-942 exhibited a higher bacterial load, more symptoms of HLB, and more growth reductions than US-812. Although we did not

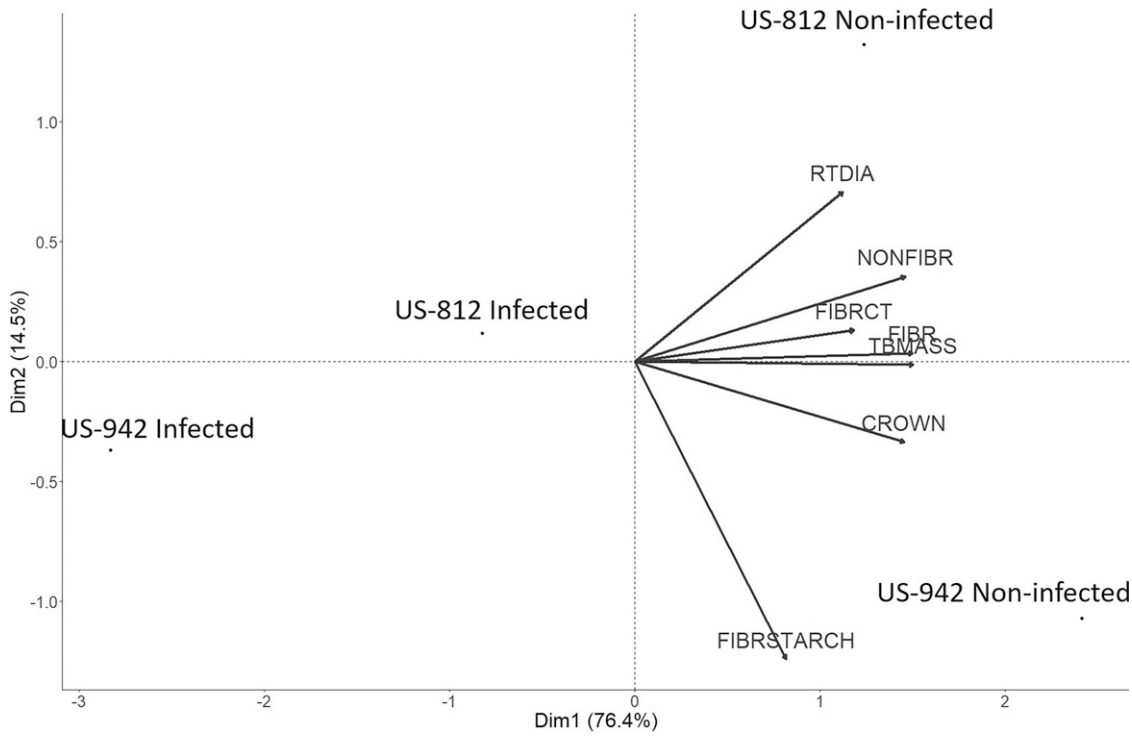

Fig. 8. Principal component analysis biplot of belowground variables. CROWN = root crown mass; Dim1 = dimension 1; Dim2 = dimension 2; FIBRCT = fibrous root cycle threshold value; FIBR = fibrous root mass; FIBRSTARCH = fibrous root starch content; NONFIBR = nonfibrous root biomass; RTDIA = rootstock trunk diameter; TBMASS = total belowground biomass.

assess this, differences in flushing patterns or flushing intensity (Carvalho et al. 2021), and therefore psyllid colonization, may have contributed to the differences in disease severity associated with the rootstock in this study. These findings reinforce that even rootstocks that are considered tolerant to HLB do not prevent tree decline under heavy HLB pressure, and that the scion generally has a greater influence on the HLB response than the rootstock (Albrecht and Bowman 2019; Tardivo et al. 2023).

To determine the extent of biomass reductions and root decline, we excavated the trees using a pneumatic arborist tool. We found extensive growth reductions in response to *C*Las infection similar to what was found during previous greenhouses experiments (Bodaghi et al. 2022a, 2022b; Bowman and Albrecht 2020). Contrary to those earlier greenhouse studies, biomass reductions were more severe for trees with US-942 than US-812. The more severe growth reductions were in accordance with the higher bacterial load measured in those trees. Overall, biomass reductions measured belowground were nearly double the reductions measured aboveground, consequently reducing the belowground-to-aboveground biomass ratio significantly. Fibrous root mass reductions were 49% despite considerably lower *C*Las titers compared with the leaves throughout the study. This disproportionally larger decline of fibrous roots compared with the other tissues raises the question of whether higher rates of ground-applied nutrients are effective for managing HLB. Recent field studies found no or only limited beneficial effects of enhanced nutrition on health and productivity of HLB-affected trees (Bassanezi et al. 2023; Esteves et al. 2021). Pustika et al. (2008) previously suggested that foliar-applied nutrients may be more beneficial for correcting foliar nutrient deficiencies in HLB-affected citrus trees.

The literature regarding *C*Las–root interactions suggests that fibrous root loss is a direct consequence of early root colonization of *C*Las (Johnson et al. 2014) or a consequence of carbohydrate starvation caused by phloem blockage and resulting metabolic disruptions in the scion (Achor et al. 2010; Aritua et al. 2013; Etxeberria et al. 2009). Kumar et al. (2018) demonstrated phloem disintegration and starch depletion in the roots, but disruptions varied by root order. Fan et al. (2013) also identified starch depletion and phloem degeneration in the roots of affected sweet orange plants but did not differentiate between root orders. However, Johnson et al. (2014) observed *C*Las colonization in most of the root system, but they did not find any phloem aberrations. Differences in the plant developmental stage, growth conditions, and, consequently, source–sink relationships are possible reasons for the differences among studies.

Contrary to the 49% fibrous root loss measured after whole root system excavations, the live root reduction measured using minirhizotrons over the course of 12 months was only 25%, and there were no rootstocks effects. In a natural field environment, minirhizotrons cover only a very small area of the whole tree root system. Our results suggest that a minirhizotron analysis is not well-suited for determining differences in root quantity in tree crops exposed to diseases or other stresses under natural field conditions. Using multiple minirhizotrons per tree may improve the results, but this is time-consuming and may negatively impact the root systems. However, a minirhizotron analysis may be suitable for capturing root growth dynamics in tree crops, as previously demonstrated (Pokhrel et al. 2021; Yao et al. 2006).

Conclusion

Exploring the effects of *C*Las infection in the field has been challenging because of the endemic nature of HLB in Florida. In this study, we used IPCs to generate noninfected and infected field-grown trees and assess the extent of HLB effects on tree physiology and growth under natural HLB-endemic conditions. Our results support those of previous studies that showed that the bacterial load in leaves is greater than that in roots. Nevertheless, compared with the growth reductions occurring aboveground, root system reductions were disproportionately larger. Compared with other tissues, fibrous roots experienced the most loss. This confirms that fibrous root loss is one of the early consequences of infection with *C*Las and contributes to the tree decline associated with HLB. However, the relationships between fibrous root loss, *C*Las colonization, phloem disintegration, and carbohydrate metabolism are not fully understood. Regardless, *C*Las infection has far-reaching consequences for tree physiology and growth, especially during the first years of field establishment. Protecting young citrus trees from psyllids, either with insecticides or with IPCs, is essential to maintain health and promote growth until they reach maturity.

References Cited

Achor DS, Etxeberria E, Wang N, Folimonova SY, Chung KR, Albrigo LG. 2010. Sequence of anatomical symptom observations in citrus affected with Huanglongbing disease. Plant Pathol J. 9(2):56–64.

Alarcón JJ, Ortuño MF, Nicolás E, Navarro A, Torrecillas A. 2006. Improving water-use efficiency of young lemon trees by shading with aluminised-plastic nets. Agric Water Manage. 82(3):387–398. https://doi.org/10.1016/j.agwat.2005.08.003.

Albrecht U, Bowman KD. 2019. Reciprocal influences of rootstock and scion citrus cultivars challenged with *Ca*. Liberibacter asiaticus. Scientia Hortic. 254:133–142. https://doi.org/10.1016/j.scienta.2019.05.010.

Albrecht U, Bowman KD. 2008. Gene expression in *Citrus sinensis* (L.) Osbeck following infection with the bacterial pathogen *Candidatus* Liberibacter asiaticus causing Huanglongbing in Florida. Plant Sci. 175(3):291–306. https://doi.org/10.1016/j.plantsci.2008.05.001.

Albrecht U, Bowman KD. 2012. Tolerance of trifoliate citrus rootstock hybrids to *Candidatus* Liberibacter asiaticus. Scientia Hortic. 147:71–80. https://doi.org/10.1016/j.scienta.2012.08.036.

Alferez F, Albrecht U, Gaire S, Batuman O, Qureshi J, Zekri M. 2021. Individual protective covers (IPCs) for young tree protection from the HLB vector, the Asian Citrus Psyllid: HS1425, 10/2021. EDIS. 2021(5). https://doi.org/10.32473/edis-hs1425-2021.

Aritua V, Achor D, Gmitter FG, Albrigo G, Wang N. 2013. Transcriptional and microscopic analyses of citrus stem and root responses to *Candidatus* Liberibacter asiaticus infection. PLoS One. 8(9):e73742. https://doi.org/10.1371/journal.pone.0073742.

Bassanezi RB, Primiano IV, Mattos D Jr, Quaggio JA, Boaretto RM, Ayres AJ, Bové JM. 2023. Calcium and magnesium input did not decrease huanglongbing progress and yield loss of sweet orange trees. Crop Prot. 172:106338. https://doi.org/10.1016/j.cropro.2023.106338.

Bodaghi S, Meyering B, Bowman KD, Albrecht U. 2022a. Different sweet orange–rootstock combinations infected by *Candidatus* Liberibacter asiaticus under greenhouse conditions: Effects on the scion. HortScience. 57(1):144–153. https://doi.org/10.21273/HORTSCI16205-21.

Bodaghi S, Pugina G, Meyering B, Bowman KD, Albrecht U. 2022b. Different sweet orange–rootstock combinations infected by *Candidatus* Liberibacter asiaticus under greenhouse conditions: Effects on the roots. HortScience. 57(1):56–64. https://doi.org/10.21273/HORTSCI16206-21.

Bové JM. 2006. Huanglongbing: A destructive, newly-emerging, century-old disease of citrus. J Plant Pathol. 88(1):7–37.

Bowman KD, McCollum G, Albrecht U. 2016a. Performance of 'Valencia' orange (*Citrus sinensis* [L.] Osbeck) on 17 rootstocks in a trial severely affected by huanglongbing. Scientia Hortic. 20:355–361. https://doi.org/10.1016/j.scienta.2016.01.019.

Bowman KD, Faulkner L, Kesinger M. 2016b. New citrus rootstocks released by USDA 2001–2010: Field performance and nursery characteristics. HortScience. 51(10):1208–1214. https://doi.org/10.21273/hortsci10970-16.

Bowman KD, Albrecht U. 2020. Rootstock influences on health and growth following *Candidatus* Liberibacter asiaticus infection in young Sweet Orange trees. Agronomy. 10(12):1907. https://doi.org/10.3390/agronomy10121907.

Braswell WE, Park J-W, Stansly PA, Kostyk BC, Louzada ES, da Graça JV, Kunta M. 2020. Root samples provide early and improved detection of *Candidatus* Liberibacter asiaticus in Citrus. Sci Rep. 10(1):16982. https://doi.org/10.1038/s41598-020-74093-x.

Brodersen C, Narciso C, Reed M, Etxeberria E. 2014. Phloem production in Huanglongbing-affected citrus trees. HortScience. 49(1):59–64. https://doi.org/10.21273/HORTSCI.49.1.59.

Budiarto R, Poerwanto R, Santosa E, Efendi D, Agusta A. 2019. Agronomical and physiological characters of kaffir lime (*Citrus hystrix* DC) seedling under artificial shading and pruning. Emir J Food Agric. 31(3):222–231. https://doi.org/10.9755/ejfa.2019.v31.i3.1920.

Carvalho EV, Cifuentes-Arenas JC, Raiol-Junior LL, Stuchi ES, Girardi EA, Lopes SA. 2021. Modeling seasonal flushing and shoot growth on different citrus scion-rootstock combinations. Scientia Hortic. 288:110358. https://doi.org/10.1016/j.scienta.2021.110358.

da Graça JV, Kunta M, Sétamou M, Rascoe J, Li W, Nakhla MK, Salas B, Bartels DW. 2015. Huanglongbing in Texas: Report on the first detections in commercial citrus. J Citrus Pathol. 2(1). https://doi.org/10.5070/C421027939.

Davidson AM, Le ST, Cooper KB, Lange E, Zwieniecki MA. 2021. No time to rest: Seasonal dynamics of non-structural carbohydrates in twigs of three Mediterranean tree species suggest

year-round activity. Sci Rep. 11(1):5181. https://doi.org/10.1038/s41598-021-83935-1.
Esteves E, Maltais-Landry G, Zambon F, Ferrarezi RS, Kadyampakeni DM. 2021. Nitrogen, calcium, and magnesium inconsistently affect tree growth, fruit yield, and juice quality of Huanglongbing-affected orange trees. HortScience. 56(10):1269–1277. https://doi.org/10.21273/HORTSCI15997-21.
Etxeberria E, Gonzalez P, Achor D, Albrigo G. 2009. Anatomical distribution of abnormally high levels of starch in HLB-affected Valencia orange trees. Physiol Mol Plant Pathol. 74(1):76–83. https://doi.org/10.1016/j.pmpp.2009.09.004.
Fan J, Chen C, Achor DS, Brlansky RH, Li Z-G, Gmitter FG Jr. 2013. Differential anatomical responses of tolerant and susceptible citrus species to the infection of '*Candidatus* Liberibacter asiaticus'. Physiol Mol Plant Pathol. 83:69–74. https://doi.org/10.1016/j.pmpp.2013.05.002.
Fan J, Chen C, Brlansky RH, Gmitter FG Jr, Li Z-G. 2010. Changes in carbohydrate metabolism in *Citrus sinensis* infected with '*Candidatus* Liberibacter asiaticus'. Plant Pathol. 59(6):1037–1043. https://doi.org/10.1111/j.1365-3059.2010.02328.x.
Gaire S, Albrecht U, Batuman O, Qureshi J, Zekri M, Alferez F. 2022. Individual protective covers (IPCs) to prevent Asian citrus psyllid and *Candidatus* Liberibacter asiaticus from establishing in newly planted citrus trees. Crop Prot. 152:105862. https://doi.org/10.1016/j.cropro.2021.105862.
Gaire S, Albrecht U, Alferez F. 2023. Effect of individual protective covers on young 'Valencia' orange (*Citrus sinensis*) tree physiology. HortScience. 58(12):1542–1549. https://doi.org/10.21273/HORTSCI17342-23.
Gottwald TR, da Graça JV, Bassanezi RB. 2007. Citrus Huanglongbing: The pathogen and its impact. Plant Health Prog. https://doi.org/10.1094/PHP-2007-0906-01-RV.
Graham J, Gottwald T, Setamou M. 2020. Status of Huanglongbing (HLB) outbreaks in Florida, California and Texas. Trop Plant Pathol. 45(3):265–278. https://doi.org/10.1007/s40858-020-00335-y.
Graham JH, Johnson EG, Gottwald TR, Irey MS. 2013. Presymptomatic fibrous root decline in citrus trees caused by Huanglongbing and potential interaction with *Phytophthora* spp. Plant Dis. 97(9):1195–1199. https://doi.org/10.1094/PDIS-01-13-0024-RE.
Halbert SE. 2005. The discovery of huanglongbing in Florida. In Proc. 2nd Intl. Citrus Canker and Huanglongbing Research Workshop. 50.
Halbert SE, Manjunath KL. 2004. Asian citrus Psyllid (Sternorrhyncha: Psyllidae) and greening disease of citrus: A literature review and assessment of risk in Florida. Fla Entomol. 87(3):330353. https://doi.org/10.1653/0015-4040(2004)087[0330:ACPSPA]2.0.CO;2.
Hall DG, Albrecht U, Bowman KD. 2016. Transmission Rates of '*Ca.* Liberibacter asiaticus' by Asian citrus Psyllid are enhanced by the presence and developmental stage of citrus flush. J Econ Entomol. 109(2):558–563. https://doi.org/10.1093/jee/tow009.
Huang CYL, Schulte EE. 1985. Digestion of plant tissue for analysis by ICP emission spectroscopy. Commun Soil Sci Plant Anal. 16(9):943–958. https://doi.org/10.1080/00103628509367657.
Johnson EG, Wu J, Bright DB, Graham JH. 2014. Association of 'Candidatus Liberibacter asiaticus' root infection, but not phloem plugging with root loss on huanglongbing-affected trees prior to appearance of foliar symptoms. Plant Pathol. 63(2):290–298. https://doi.org/10.1111/ppa.12109.
Kim J-S, Sagaram US, Burns JK, Li J-L, Wang N. 2009. Response of sweet orange (*Citrus sinensis*) to '*Candidatus* Liberibacter asiaticus' infection: Microscopy and microarray analyses. Phytopathology. 99(1):50–57. https://doi.org/10.1094/PHYTO-99-1-0050.
Kumar N, Kiran F, Etxeberria E. 2018. Huanglongbing-induced anatomical changes in citrus fibrous root orders. HortScience. 53(6):829–837. https://doi.org/10.21273/HORTSCI12390-17.
Lamari, L. 2008. Assess 2.0 image analysis software for plant disease quantification. American Phytopathological Society, St. Paul, MN, USA.
Lê S, Josse J, Husson F. 2008. FactoMineR: An R package for multivariate analysis. J Stat Softw. 25:1–18. https://doi.org/10.18637/jss.v025.i01.
Leyva A, Quintana A, Sánchez M, Rodríguez EN, Cremata J, Sánchez JC. 2008. Rapid and sensitive anthrone–sulfuric acid assay in microplate format to quantify carbohydrate in biopharmaceutical products: Method development and validation. Biologicals. 36(2):134–141. https://doi.org/10.1016/j.biologicals.2007.09.001.
Li W, Hartung JS, Levy L. 2006. Quantitative real-time PCR for detection and identification of *Candidatus* Liberibacter species associated with citrus huanglongbing. J Microbiol Methods. 6(1):104–115. https://doi.org/10.1016/j.mimet.2005.10.018.
Lugojan C, Ciulca S. 2011. Evaluation of relative water content in winter wheat. J Hortic For Biotechnol. 15(2):173–177.
Mahmood A, Hu Y, Tanny J, Asante EA. 2018. Effects of shading and insect-proof screens on crop microclimate and production: A review of recent advances. Scientia Hortic. 241:241–251. https://doi.org/10.1016/j.scienta.2018.06.078.
Morgan KT, Kadyampakeni DM. 2020. Nutrition of Florida citrus trees (3rd ed). Soil and leaf tissue testing, SL458, EDIS 2020. University of Florida/IFAS, Gainesville, FL, USA.
Pegoraro E, Rey A, Barron-Gafford G, Monson R, Malhi Y, Murthy R. 2005. The interacting effects of elevated atmospheric CO_2 concentration, drought and leaf-to-air vapour pressure deficit on ecosystem isoprene fluxes. Oecologia. 146(1):120–129. https://doi.org/10.1007/s00442-005-0166-5.
Pokhrel S, Meyering B, Bowman KD, Albrecht U. 2021. Horticultural attributes and root architectures of field-grown 'Valencia' trees grafted on different rootstocks propagated by seed, cuttings, and tissue culture. HortScience. 56(2):163–172. https://doi.org/10.21273/HORTSCI15507-20.
Pustika AB, Subandiyah S, Holford P, Beattie GAC, Iwanami T, Masaoka Y. 2008. Interactions between plant nutrition and symptom expression in mandarin trees infected with the disease huanglongbing. Australas Plant Dis Notes. 3(1):112–115. https://doi.org/10.1007/BF03211261.
R Core Team. 2021. R: A language and environment for statistical computing. R Foundation for Statistical Computing, Vienna, Austria. https://www.R-project.org/.
Raiol-Junior LL, Cifuentes-Arenas JC, de Carvalho EV, Girardi EA, Lopes SA. 2021. Evidence that '*Candidatus* Liberibacter asiaticus' moves predominantly toward new tissue growth in citrus plants. Plant Dis. 105(1):34–42. https://doi.org/10.1094/PDIS-01-20-0158-RE.
Rosson B. 2022. Citrus Budwood Annual Report 2021-2022. Florida Department of Agriculture and Consumer Services. https://ccmedia.fdacs.gov/content/download/108719/file/2021-2022-citrus-budwood-annual-report.pdf.
Shin K, van Bruggen AHC. 2018. *Bradyrhizobium* isolated from huanglongbing (HLB) affected citrus trees reacts positively with primers for *Candidatus* Liberibacter asiaticus. Eur J Plant Pathol. 151:291–306. https://doi.org/10.1007/s10658-017-1372-9.
Schindelin J, Arganda-Carreras I, Frise E, Kaynig V, Longair M, Pietzsch T, Preibisch S, Rueden C, Saalfeld S, Schmid B, Tinevez J-Y, White DJ, Hartenstein V, Eliceiri K, Tomancak, Cardona A. 2012. Fiji: an open-source platform for biological-image analysis. Nature Methods. 9(7):676–682. https://doi.org/10.1038/nmeth.2019.
Sneath PH, Sokal RR. 1973. Numerical taxonomy. The principles and practice of numerical classification (1st ed). WH Freeman, San Francisco, CA, USA.
Syvertsen J, Levy Y. 2005. salinity interactions with other abiotic and biotic stresses in citrus. HortTechnology. 15(1):100–103. https://doi.org/10.21273/HORTTECH.15.1.0100.
Sweeney RA. 1989. Generic combustion method for determination of crude protein in feeds: Collaborative study. J Assoc Off Anal Chem. 72(5):770–774.
Tardivo C, Qureshi J, Bowman KD, Albrecht U. 2023. relative influence of rootstock and scion on Asian citrus Psyllid infestation and *Candidatus* Liberibacter asiaticus colonization. HortScience. 58(4):395–403. https://doi.org/10.21273/HORTSCI17039-22.
Tixier A, Sperling O, Orozco J, Lampinen B, Amico Roxas A, Saa S, Earles JM, Zwieniecki MA. 2017. Spring bud growth depends on sugar delivery by xylem and water recirculation by phloem Münch flow in *Juglans regia.* Planta. 246(3):495–508. https://doi.org/10.1007/s00425-017-2707-7.
Vincent C, Wang Y, Killiny N. 2023. Increase yield with shade. Citrus industry, tip of the week. https://citrusindustry.net/2023/10/17/increase-yield-with-shade/. [accessed 12 Dec 2023].
Yao S, Merwin IA, Brown MG. 2006. Root dynamics of apple rootstocks in a replanted orchard. HortScience. 41(5):1149–1155. https://doi.org/10.21273/HORTSCI.41.5.1149.
Yu Q, Dai F, Russo R, Guha A, Pierre M, Zhuo X, Wang YZ, Vincent C, Gmitter FG. 2023. Phenotypic and genetic variation in morpho-physiological traits in Huanglongbing-affected mandarin hybrid populations. Plants. 12(1):42. https://doi.org/10.3390/plants12010042.